The relaxation dynamics of spin $I=1$ nuclei with a static quadrupolar coupling and a radio-frequency field

J. R. C. van der Maarel
Department of Physical and Macromolecular Chemistry, Gorlaeus Laboratories, Leiden University, P. O. Box 9502, 2300 RA Leiden, The Netherlands

(Received 18 February 1993; accepted 29 June 1993)

The dynamics of spin $I=1$ nuclei in a radio-frequency (rf) field and with both a static and fluctuating quadrupolar interaction are discussed. Approximate expressions of the relaxation rates are derived under the assumption that the linewidths are much smaller than the characteristic line-splittings. The conventional spin-lock relaxation rate increases with increasing ratio of the spin-lock field strength and static quadrupolar coupling ω_1/ω_Q and is sensitive to the spectral density at frequency $\sqrt{\omega_Q^2+4\omega_1^2}$. The rate shows a maximum in the presence of low frequency molecular motion. Some experiments are performed on a deuterium spin probe in a low molecular weight liquid crystal. The creation of multipolar states by continuous rf irradiation is demonstrated.

INTRODUCTION

The measurement of the magnetic relaxation rates of spin $I=1$ nuclei, e.g., ^{2}H and ^{14}N, is an important method to investigate the molecular reorientation dynamics in condensed matter. For these chemically bound nuclei, the dominant relaxation mechanism is the intramolecular quadrupolar interaction. In macroscopically oriented systems, such as liquid crystals, there might be a residual static quadrupolar coupling. The latter coupling causes the characteristic line-splitting of the spin $I=1$ resonance.

The Fourier components (spectral density) of the correlation function of the fluctuating quadrupolar interaction tensor can be studied using (selective) inversion recovery and/or Jeener–Broekaert pulse sequences.[1,2] Transverse relaxation rates are sensitive to the value of the spectral density at zero frequency, and, hence, to low frequency molecular motion. However, the measurement of transverse relaxation rates may be complicated due to additional dephasing contributions. These contributions include translation diffusion and a possible inhomogeneity in static quadrupolar coupling. These effects can be removed by spin-locking the magnetization in the rotating frame using a radio-frequency (rf) field.

In the absence of a static quadrupolar coupling, the theoretical framework to study nuclear magnetic resonance (NMR) relaxation of quadrupolar spin 1 and 3/2 under (pulsed) spin-locking have been provided by Blicharski[3] and the present author,[4,5] respectively. The spin-lock relaxation rate is sensitive to the spectral density at two times the Larmor frequency with respect to the spin-lock field $2\gamma B_1$, with B_1 the spin-lock field strength. The latter frequency is typically of the order kHz. The low frequency behavior of the spectral density can be probed by adopting the transmitter power level. The dynamics of spin $I=1$ nuclei in a rf field and with a static quadrupolar coupling, but under the neglect of relaxation, have been evaluated by Bowden, Hutchinson, and Separovic[6] and Vega and Pines.[7] In the present contribution, the time-evolution of the density operator in the presence of a rf field and both a static and fluctuating quadrupolar interaction will be discussed.

Following Bowden *et al.*,[6] the density operator is expressed in an irreducible tensor operator basis. The master equation decomposes into two sets of coupled differential equations. One set is relevant for $T_{1\rho}$ experiments, in which the magnetization is spin-locked along the rf field in the rotating frame. The second set describes $T_{2\rho}$ relaxation of magnetization perpendicular to the rf field. Approximate solutions are derived under the assumption that the linewidths are much smaller than the characteristic line-splittings. Some experiments are performed on a deuterium spin probe in a low molecular weight liquid crystal.

DIFFERENTIAL EQUATIONS

In this contribution the spin density operator as well as the Hamiltonian are expressed in terms of irreducible tensor operators.[8] The relevant spin operators for $I=1$ are summarized in Table I. The unit tensor operators, indicated with the cap hat, fulfill the normalization $\mathrm{Tr}\{\hat{T}^\dagger_{lm}\hat{T}_{l'm'}\}=\delta_{ll'}\delta_{mm'}$ with $\hat{T}^\dagger_{lm}=(-1)^m\hat{T}_{l-m}$. Symmetric and antisymmetric combinations are defined according to

$$T_{lp}(s)=1/\sqrt{2}(T_{l-p}+T_{lp}),$$
$$T_{lp}(a)=1/\sqrt{2}(T_{l-p}-T_{lp}), \tag{1}$$

respectively. For unit tensor operators these combinations are analogously defined. The commutation relations are conveniently tabulated in Ref. 9.

The spin system evolves under the simultaneous action of the Zeeman, static quadrupolar, spin-lock, and fluctuating quadrupolar Hamiltonian. All calculations reported here refer to the Larmor frequency rotating frame (indicated by the asterisk). In this representation, the Zeeman Hamiltonian $H_z=\omega_O T_{10}$ vanishes. The static quadrupolar Hamiltonian commutes with the Zeeman Hamiltonian and is given by

$$H^*_{QS}=H_{QS}=\omega_Q/3[3I_z^2-I(I+1)]=\sqrt{(2/3)}\omega_Q T_{20}, \tag{2}$$

 0021-9606/93/99(8)/5646/8/$6.00

TABLE I. Relevant irreducible tensor operators for spin $I=1$ (Ref. 8).[a]

$T_{10}=I_z$	$T_{20}=1/\sqrt{6}[3I_z^2-I(I+1)]$
$T_{1\pm1}=\mp1/\sqrt{2}I_\pm$	$T_{2\pm1}=\mp1/2\{I_zI_\pm+I_\pm I_z\}$
	$T_{2\pm2}=1/2I_\pm^2$

[a]For spin $I=1$ the unit tensor operators are defined according to $\hat{T}_{2m}=T_{2m}$, $\hat{T}_{1m}=1/\sqrt{2}T_{1m}$.

where ω_Q denotes the static quadrupolar coupling parameter. The spin-lock field is applied exactly on resonance along the x axis with field strength $\omega_1=-\gamma B_1$. In the Larmor frequency rotating frame the spin-lock Hamiltonian becomes time-independent and reads

$$H_1^*=\omega_1 I_x=\omega_1 T_{11}(a). \tag{3}$$

The zero average fluctuating quadrupolar interaction Hamiltonian becomes

$$H_{QF}^*(t)=C\sum_{m=-2}^{2}(-1)^m T_{2m}\exp(im\omega_Q t) \times[F_{2-m}(t)-\langle F_{2-m}\rangle] \tag{4}$$

with $C=\sqrt{(3/2)}eQ/\hbar$. The electric field gradient tensor components (in the laboratory frame defined) are given by

$$F_{20}=1/2V_{zz},$$
$$F_{2\pm1}=\mp1/\sqrt{6}(V_{xz}\pm iV_{yz}), \tag{5}$$
$$F_{2\pm2}=1/(2\sqrt{6})(V_{xx}-V_{yy}\pm 2iV_{xy})$$

and $\langle F_{2m}\rangle$ denotes the average value.

The static quadrupolar as well as the spin-lock Hamiltonian are time-independent (i.e., in the Larmor frequency rotating frame). The fluctuating quadrupolar interaction induces relaxation. The time-evolution of the density operator under a static Hamiltonian H_S^* and a fluctuating part $H_{QF}^*(t)$ is given by the master equation[10]

$$\frac{d\sigma^*}{dt}=-i[H_S^*,\sigma^*]+f(\sigma^*) \tag{6}$$

with

$$H_S^*=H_1^*+H_{QS}^* \tag{7}$$

and the relaxation term

$$f(\sigma^*)=-\int_0^\infty\langle[H_{QF}^*(t),[\exp(-iH_S^*\tau) \times H_{QF}^*(t-\tau)\exp(iH_S^*\tau),\sigma^*(t)]]\rangle d\tau. \tag{8}$$

The validity of this equation has been discussed by Abragam.[10] Please note the presence of H_S^* in the relaxation contribution.

The evolution due to the first term in Eq. (6) (i.e., under neglect of relaxation) can be solved in analytical form.[6,7] The formal solution reads $\sigma^*(t)=\exp(-iH_S^*t)\sigma^*(0)\exp(iH_S^*t)$. However, relaxation effects are most easily taken into account by using the differential form. With the Hamiltonians Eqs. (2) and (3), this first term becomes

$$\frac{d\sigma^*}{dt}=-i[\sqrt{(2/3)}\omega_Q T_{20}+\omega_1 T_{11}(a),\sigma^*]. \tag{9}$$

Now, the density operator is expanded in an irreducible tensor operator basis. Differential equations are derived which couple the $\hat{T}_{lm}$. These equations can be decoupled and subsequently integrated.

The density operator σ^* is expressed in the operator set $\hat{T}_{20}$, $\hat{T}_{11}(a)$, $\hat{T}_{21}(s)$, $\hat{T}_{22}(s)$, $\hat{T}_{10}$, $\hat{T}_{11}(s)$, $\hat{T}_{21}(a)$, and $\hat{T}_{22}(a)$. In principle, all these components are experimentally accessible using $T_{1\rho}$ and $T_{2\rho}$ experiments, possibly supplemented with phase cycling and/or coherence transfer. Some examples will be discussed below. The longitudinal magnetization is proportional to $\hat{T}_{10}$. The spin-locked magnetization along B_1 (i.e., the x-axis) is proportional to $\hat{T}_{11}(a)$, whereas the component along the y-axis perpendicular to the rf field is proportional to $\hat{T}_{11}(s)$. There are two additional single-quantum coherences $\hat{T}_{21}(s)$ and $\hat{T}_{21}(a)$. The double-quantum coherences are given by $\hat{T}_{22}(s)$ and $\hat{T}_{22}(a)$. Finally, $\hat{T}_{20}$ denotes the quadrupolar spin polarization.

With the commutation relations,[9] Eq. (9) reduces to two sets of coupled differential equations. For the first set, one obtains

$$\frac{d}{dt}\begin{pmatrix}\hat{T}_{20}\\ \hat{T}_{11}(a)\\ \hat{T}_{21}(s)\\ \hat{T}_{22}(s)\end{pmatrix}=\begin{pmatrix}0 & 0 & -\sqrt{3}i\omega_1 & 0\\ 0 & 0 & i\omega_Q & 0\\ -\sqrt{3}i\omega_1 & i\omega_Q & 0 & -i\omega_1\\ 0 & 0 & -i\omega_1 & 0\end{pmatrix} \times\begin{pmatrix}\hat{T}_{20}\\ \hat{T}_{11}(a)\\ \hat{T}_{21}(s)\\ \hat{T}_{22}(s)\end{pmatrix}, \tag{10}$$

and for the second set

$$\frac{d}{dt}\begin{pmatrix}\hat{T}_{10}\\ \hat{T}_{11}(s)\\ \hat{T}_{21}(a)\\ \hat{T}_{22}(a)\end{pmatrix}=\begin{pmatrix}0 & -i\omega_1 & 0 & 0\\ -i\omega_1 & 0 & i\omega_Q & 0\\ 0 & i\omega_Q & 0 & -i\omega_1\\ 0 & 0 & -i\omega_1 & 0\end{pmatrix} \times\begin{pmatrix}\hat{T}_{10}\\ \hat{T}_{11}(s)\\ \hat{T}_{21}(a)\\ \hat{T}_{22}(a)\end{pmatrix}. \tag{11}$$

The first set contains the component $\hat{T}_{11}(a)$ and is relevant for $T_{1\rho}$ experiments. The second set contains $\hat{T}_{10}$ and $\hat{T}_{11}(s)$. These components are perpendicular to the rf field and are relevant for $T_{2\rho}$ experiments.

The matrices in Eqs. (10) and (11) can be diagonalized and subsequently integrated in analytical form. For the matrix in Eq. (10), the eigenvalues and corresponding eigenoperators are, respectively,

TABLE II. Time-dependence of the irreducible tensor operators due to H_S^*.

U	$\exp(-iH_S^*t)\,U\exp(iH_S^*t)$
$\hat{T}_{20}$	$\sqrt{3}\omega_1\omega_Q[1-\cos(k_1t)]/k_1^2\hat{T}_{11}(a)+\{\omega_Q^2+\omega_1^2[1+3\cos(k_1t)]\}/k_1^2\hat{T}_{20}$ $-i\sqrt{3}\omega_1\sin(k_1t)/k_1\hat{T}_{21}(s)+\sqrt{3}\omega_1^2[\cos(k_1t)-1]/k_1^2\hat{T}_{22}(s)$
$\hat{T}_{11}(a)$	$[\omega_Q^2\cos(k_1t)+4\omega_1^2]/k_1^2\hat{T}_{11}(a)+\sqrt{3}\omega_1\omega_Q[1-\cos(k_1t)]/$ $k_1^2\hat{T}_{20}+i\omega_Q\sin(k_1t)/k_1\hat{T}_{21}(s)+\omega_1\omega_Q[1-\cos(k_1t)]/k_1^2\hat{T}_{22}(s)$
$\hat{T}_{21}(s)$	$i\omega_Q\sin(k_1t)/k_1\hat{T}_{11}(a)-i\sqrt{3}\omega_1\sin(k_1t)/k_1\hat{T}_{20}$ $+\cos(k_1t)\hat{T}_{21}(s)-i\omega_1\sin(k_1t)/k_1\hat{T}_{22}(s)$
$\hat{T}_{22}(s)$	$\omega_1\omega_Q[1-\cos(k_1t)]/k_1^2\hat{T}_{11}(a)+\sqrt{3}\omega_1^2[\cos(k_1t)-1]/k_1^2\hat{T}_{20}$ $-i\omega_1\sin(k_1t)/k_1\hat{T}_{21}(s)+(1-\{\omega_1^2[1-\cos(k_1t)]\}/k_1^2)\hat{T}_{22}(s)$
$\hat{T}_{10}$	$[k_2\cos(k_3t)-k_3\cos(k_2t)]/k_1\hat{T}_{10}+i\omega_1[\sin(k_3t)-\sin(k_2t)]/k_1\hat{T}_{11}(s)$ $+\omega_1[\cos(k_3t)-\cos(k_2t)]/k_1\hat{T}_{21}(a)+i[k_2\sin(k_3t)-k_3\sin(k_2t)]/k_1\hat{T}_{22}(a)$
$\hat{T}_{11}(s)$	$i\omega_1[\sin(k_3t)-\sin(k_2t)]/k_1\hat{T}_{10}+[k_2\cos(k_2t)-k_3\cos(k_3t)]/k_1\hat{T}_{11}(s)$ $+i[k_2\sin(k_2t)-k_3\sin(k_3t)]/k_1\hat{T}_{21}(a)+\omega_1[\cos(k_3t)-\cos(k_2t)]/k_1\hat{T}_{22}(a)$
$\hat{T}_{21}(a)$	$\omega_1[\cos(k_3t)-\cos(k_2t)]/k_1\hat{T}_{10}+i[k_2\sin(k_2t)-k_3\sin(k_3t)]/k_1\hat{T}_{11}(s)$ $+[k_2\cos(k_2t)-k_3\cos(k_3t)]/k_1\hat{T}_{21}(a)+i\omega_1[\sin(k_3t)-\sin(k_2t)]/k_1\hat{T}_{22}(a)$
$\hat{T}_{22}(a)$	$i[k_2\sin(k_3t)-k_3\sin(k_2t)]/k_1\hat{T}_{10}+\omega_1[\cos(k_3t)-\cos(k_2t)]/k_1\hat{T}_{11}(s)$ $+i\omega_1[\sin(k_3t)-\sin(k_2t)]/k_1\hat{T}_{21}(a)+[k_2\cos(k_3t)-k_3\cos(k_2t)]/k_1\hat{T}_{22}(a)$

$$
\begin{aligned}
&0, \quad A_1=\hat{T}_{20}-\sqrt{3}\hat{T}_{22}(s)\\
&0, \quad A_2=\omega_1\hat{T}_{11}(a)+\omega_Q\hat{T}_{22}(s),\\
&\pm ik_1, \quad A_{\pm 3}=\sqrt{3}\omega_1\hat{T}_{20}-\omega_Q\hat{T}_{11}(a)\mp k_1\hat{T}_{21}(s)\\
&\qquad\qquad +\omega_1\hat{T}_{22}(s),
\end{aligned}
\tag{12}
$$

and for Eq. (11), one obtains

$$
\begin{aligned}
&\pm ik_2, \quad B_{\pm 1}=\omega_1\hat{T}_{10}\mp k_2\hat{T}_{11}(s)-k_2\hat{T}_{21}(a)\\
&\qquad\qquad \pm\omega_1\hat{T}_{22}(a)\\
&\pm ik_3, \quad B_{\pm 2}=\omega_1\hat{T}_{10}\mp k_3\hat{T}_{11}(s)-k_3\hat{T}_{21}(a)\\
&\qquad\qquad \pm\omega_1\hat{T}_{22}(a)
\end{aligned}
\tag{13}
$$

with $k_1=\sqrt{(\omega_Q^2+4\omega_1^2)}$, $k_2=(\omega_Q+k_1)/2$, and $k_3=(\omega_Q-k_1)/2$. Please note that due to the fact that A_1 and A_2 have the same eigenvalue, any linear combination of these operators represents an eigenoperator. The resulting evolution of the tensor operators under the action of the static Hamiltonian is summarized in Table II. In the limit $\omega_Q\to 0$, these results represent a tensor rotation about the x-axis, which is related to symmetric and antisymmetric combinations of the Wigner rotation matrix elements.

The results in Table II agree with the results reported by Bowden, Hutchinson, and Separovic[6] using a similar operator basis and Vega and Pines[7] using the fictitious spin 1/2 formalism. In the present formalism, relaxation effects can easily be incorporated due to the fact that the differential form has been used. For this purpose, Eqs. (10) and (11) have to be supplemented with the relaxation contribution Eq. (8). Now, the differential equations which couple the $\hat{T}_{lm}$ cannot be solved in analytical form. However, approximate solutions can be derived under the assumption that the linewidths are much smaller than the characteristic frequencies k_i.

With the fluctuating Hamiltonian Eq. (4) and neglect of (nonsecular) terms oscillating with a multiple of the Larmor frequency, Eq. (8) reads

$$
\begin{aligned}
f(\sigma^*)=-C^2\sum_{m=-2}^{2}\int_0^\infty &[T_{2m},[\exp(-iH_S^*\tau)T_{2m}^\dagger\\
&\times\exp(iH_S^*\tau),\sigma^*(t)]]\\
&\times\langle[F_{2m}^*(t)-\langle F_{2m}^*\rangle][F_{2m}(t-\tau)-\langle F_{2m}\rangle]\rangle\\
&\times\exp(im\omega_O\tau)d\tau.
\end{aligned}
\tag{14}
$$

The double commutator can be calculated using the results in Table II. The relaxation term reduces to combinations of the spectral density function at a number of frequencies. The real part of the spectral density function is defined according to

$$
\begin{aligned}
J_m(\omega)=C^2 1/2\int_{-\infty}^{\infty}&\langle[F_{2m}^*(t)-\langle F_{2m}^*\rangle]\\
&\times[F_{2m}(t-\tau)-\langle F_{2m}\rangle]\rangle\exp(i\omega\tau)d\tau.
\end{aligned}
\tag{15}
$$

The imaginary part induces a very small second order frequency shift and is neglected.[10]

The relaxation contribution includes terms proportional to $J_m(m\omega_O\pm k_i)$, where the shift $\pm k_i$ is due to the presence of H_S^*. The Larmor frequency is generally much larger than anyone of the frequencies k_i. For $m\neq 0$, the difference between $J_m(m\omega_O\pm k_i)$ and $J_m(m\omega_O)$ is immaterial, and, hence, H_S^* in Eq. (14) can be neglected. The term with $m=0$ reduces to combinations of the spectral density at frequencies k_1 and zero. These spectral densities are

TABLE III. The spin operator double commutator for $m=0$.

σ^*	$[T_{20},[\exp(-iH_S^*\tau)T_{20}\exp(iH_S^*\tau),\sigma^*]]$
$\hat{T}_{20}$	$3/2\sqrt{3}\omega_1\omega_Q[\cos(k_1\tau)-1]/k_1^2\hat{T}_{11}(a)+3/2\sqrt{3}i\omega_1\sin(k_1\tau)/k_1\hat{T}_{21}(s)$
$\hat{T}_{11}(a)$	$3/2[\omega_Q^2+4\omega_1^2\cos(k_1\tau)]/k_1^2\hat{T}_{11}(a)$
$\hat{T}_{21}(s)$	$3/2[\omega_Q^2+4\omega_1^2\cos(k_1\tau)]/k_1^2\hat{T}_{21}(s)$
$\hat{T}_{22}(s)$	$3/2\omega_1\omega_Q[\cos(k_1\tau)-1]/k_1^2\hat{T}_{11}(a)+3/2i\omega_1\sin(k_1\tau)/k_1\hat{T}_{21}(s)$
$\hat{T}_{10}$	$3/2\omega_1\omega_Q[\cos(k_1\tau)-1]/k_1^2\hat{T}_{21}(a)+3/2i\omega_1\sin(k_1\tau)/k_1\hat{T}_{11}(s)$
$\hat{T}_{11}(s)$	$3/2\{\omega_Q^2+2\omega_1^2[1+\cos(k_1\tau)]\}/k_1^2\hat{T}_{11}(s)$
$\hat{T}_{21}(a)$	$3/2\{\omega_Q^2+2\omega_1^2[1+\cos(k_1\tau)]\}/k_1^2\hat{T}_{21}(a)$
$\hat{T}_{22}(a)$	$3/2\omega_1\omega_Q[\cos(k_1\tau)-1]/k_1^2\hat{T}_{11}(s)+3/2i\omega_1\sin(k_1\tau)/k_1\hat{T}_{21}(a)$

sensitive to slow motion and are the main object of this study. Accordingly, for $m=0$ $f(\sigma^*)$ has to be fully evaluated.

The spin operator double commutator $[T_{20},[\exp(-iH_S^*\tau)T_{20}\exp(iH_S^*\tau),\sigma^*]]$ (i.e., for $m=0$) is evaluated using the results of Table II. For the different basis operators, this double commutator is set out in Table III. With these results, together with Eqs. (10),(11),(14),(15), and the neglect of H_S^* in the $m=\pm1$ and ±2 contributions, Eq. (6) reduces to the coupled differential equations

$$\frac{d}{dt}\begin{pmatrix}\hat{T}_{20}\\ \hat{T}_{11}(a)\\ \hat{T}_{21}(s)\\ \hat{T}_{22}(s)\end{pmatrix}=\begin{pmatrix}-\alpha_1 & \sqrt{3}\beta & -\sqrt{3}i\omega_1 & 0\\ 0 & -\alpha_2 & i\omega_Q & 0\\ -\sqrt{3}i\omega_1 & i\omega_Q & -\alpha_3 & -i\omega_1\\ 0 & \beta & -i\omega_1 & -\alpha_4\end{pmatrix}\times\begin{pmatrix}\hat{T}_{20}\\ \hat{T}_{11}(a)\\ \hat{T}_{21}(s)\\ \hat{T}_{22}(s)\end{pmatrix}, \tag{16}$$

$$\frac{d}{dt}\begin{pmatrix}\hat{T}_{10}\\ \hat{T}_{11}(s)\\ \hat{T}_{21}(a)\\ \hat{T}_{22}(a)\end{pmatrix}=\begin{pmatrix}-\gamma_1 & -i\omega_1 & \beta & 0\\ -i\omega_1 & -\gamma_2 & i\omega_Q & 0\\ 0 & i\omega_Q & -\gamma_3 & -i\omega_1\\ 0 & \beta & -i\omega_1 & -\gamma_4\end{pmatrix}\times\begin{pmatrix}\hat{T}_{10}\\ \hat{T}_{11}(s)\\ \hat{T}_{21}(a)\\ \hat{T}_{22}(a)\end{pmatrix}, \tag{17}$$

where

$$\begin{aligned}
\alpha_1&=3J_1(\omega_O),\\
\alpha_2&=3/2[\omega_Q^2J_0(0)+4\omega_1^2J_0(k_1)]/k_1^2+5/2J_1(\omega_O)\\
&\quad+J_2(2\omega_O),\\
\alpha_3&=3/2[\omega_Q^2J_0(0)+4\omega_1^2J_0(k_1)]/k_1^2+1/2J_1(\omega_O)\\
&\quad+J_2(2\omega_O),\\
\alpha_4&=J_1(\omega_O)+2J_2(2\omega_O),\\
\gamma_1&=J_1(\omega_O)+4J_2(2\omega_O),\\
\gamma_2&=3/2\{\omega_Q^2J_0(0)+2\omega_1^2[J_0(0)+J_0(k_1)]\}/k_1^2\\
&\quad+5/2J_1(\omega_O)+J_2(2\omega_O),\\
\gamma_3&=3/2\{\omega_Q^2J_0(0)+2\omega_1^2[J_0(0)+J_0(k_1)]\}/k_1^2\\
&\quad+1/2J_1(\omega_O)+J_2(2\omega_O),\\
\gamma_4&=J_1(\omega_O)+2J_2(2\omega_O),\\
\beta&=3/2\omega_1\omega_Q[J_0(0)-J_0(k_1)]/k_1^2.
\end{aligned} \tag{18}$$

Apart from the conventional spectral densities $J_0(0)$, $J_1(\omega_O)$, and $J_2(2\omega_O)$ the relaxation matrix contains the spectral density at frequency k_1: $J_0(k_1)$.

The final differential equations governing the time-dependence of the basis operators under the action of the static Hamiltonian and relaxation effects are given by Eqs. (16) and (17). When relaxation effects are included, the master equation can only be integrated in analytical form in the two limiting cases $\omega_1=0$ and/or $\omega_Q=0$.

In the absence of a spin-lock field ($\omega_1=0$, $k_1=\omega_Q$) the relaxation contribution becomes diagonal ($\beta=0$). The relaxation rates agree with the results of Jacobsen, Bildsøe, and Schaumburg.[11] The ω_Q dependence in the rates Eq. (18) vanishes. This is due to the fact that the static quadrupolar Hamiltonian Eq. (2) commutes with T_{20} in the spin operator double commutator. The difference in relaxation behavior of the symmetric and antisymmetric tensor combinations vanishes as well. This is related to the invariance of the spin system under a rotation about the z-axis. The differential equations can be solved in analytical form and have been reviewed by Vold.[1]

In the absence of a static quadrupolar interaction ($\omega_Q=0$, $k_1=2\omega_1$) the spin-locked magnetization $[\hat{T}_{11}(a)]$ is decoupled from any other $\hat{T}_{lm}$, and, hence, relaxes according to a single exponential[3]

$$\hat{T}_{11}(a)\rightarrow\exp\{-[3/2J_0(2\omega_1)+5/2J_1(\omega_O)+J_2(2\omega_O)]t\}\hat{T}_{11}(a). \tag{19}$$

The components perpendicular to the rf field axis, i.e., $\hat{T}_{10}$ and $\hat{T}_{11}(s)$, are coupled. The relaxation behavior (referred to as $T_{2\rho}$) can be solved in analytical form. For a sufficiently intense rf field they relax with the averaged rate $(\gamma_1+\gamma_2)/2$ and oscillate with frequency $\omega_1/2\pi$. However, these signals have little practical value due to line-broadening effects caused by B_1 field inhomogeneity. The other operators are not accessible.

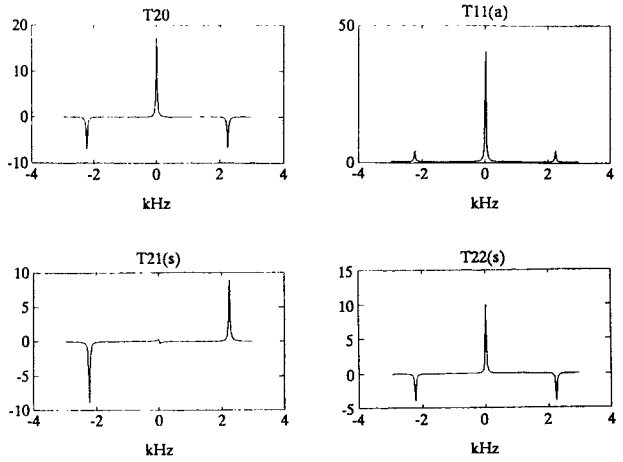

FIG. 1. Simulated spectra resulting from the Fourier transform of the numerically solved time-evolution Eq. (16). The density operator is prepared in a $\hat{T}_{11}(a)$ state by an initial $(\pi/2)_y$ pulse ($T_{1\rho}$ experiments). The detected coherences are indicated in the figure. The spectral densities are calculated using an exponential correlation function with a correlation time $\tau_c=0.1$ ms and a coupling constant $e^2qQ/h=1$ kHz (see text). The other parameters are $\omega_Q/2\pi=\omega_1/2\pi=1$ kHz.

In the simultaneous presence of a spin-lock field and a static quadrupolar coupling the master equation cannot be solved in analytical form. Numerically simulated spectra are displayed in Figs. 1 and 2. The spectra in Fig. 1 refer to $T_{1\rho}$ experiments in which the density operator is prepared in a $\hat{T}_{11}(a)$ state by a $(\pi/2)_y$ preparation pulse. The spectra in Fig. 2 refer to $T_{2\rho}$ experiments in which the initial density operator is proportional to the equilibrium $\hat{T}_{10}$ state. The initial density operator evolves into the different coherences indicated in the figures. The spectra are the Fourier transform of the numerically solved time-evolution Eqs. (16) and (17) with the appropriate initial conditions. The $T_{1\rho}$ spectra show a central line and one satellite pair [the central component of the $\hat{T}_{21}(s)$ coherence is insignificant], whereas the spectra in Fig. 2 show two satellite

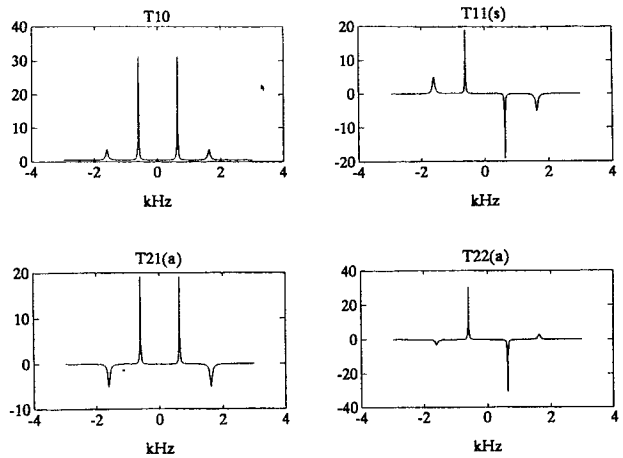

FIG. 2. Same as Fig. 1, but with the initial density operator in the equilibrium $\hat{T}_{10}$ state [$T_{2\rho}$ experiments, Fourier transform of the numerically solved time-evolution Eq. (17)].

pairs. Satellites are liable to inhomogeneous line-broadening due to B_1 inhomogeneity and/or a possible distribution in ω_Q. Accordingly, in the $T_{1\rho}$ spectra the central line is designated for relaxation studies.

APPROXIMATE SOLUTIONS

Although a numerical integration procedure is feasible, approximate solutions might be convenient. These solutions can be obtained under the assumption that the linewidths are much smaller than the frequencies k_i. In this situation, the eigenoperators in Eqs. (12) and (13) are still approximate eigenoperators. The resonance positions (i.e., the frequencies k_i) and relative intensities are given by the results in Table II.

To obtain approximate values of the relaxation rates, Eqs. (16) and (17) have to be transformed to the approximate eigenoperator representation. The operators $A_{\pm 3}$, $B_{\pm 1}$, and $B_{\pm 2}$ oscillate with frequencies $\pm k_1$, $\pm k_2$, and $\pm k_3$, respectively. If the linewidths are much smaller than the frequencies k_i these operators relax independently and are decoupled from any other eigenoperator. The operators A_1 and A_2 do not oscillate [any linear combination represents an eigenoperator of Eq. (10)]. Accordingly, these operators are coupled (by the relaxation contribution) and some further simplifying assumptions are necessary.

For decoupled operators, the relaxation rates are given by the real part of the diagonal elements of the master equation in the approximate eigenoperator representation. The imaginary part represents the frequencies. The diagonal elements are given by

$$\begin{aligned} A_1&: \ 3\omega_1^2/k_1^2(\alpha_1-\alpha_4)-\alpha_1, \\ A_2&: \ -4\omega_1^2/k_1^2(\alpha_2-\alpha_4)-\alpha_4+4\omega_Q\omega_1/k_1^2\beta, \\ A_{\pm 3}&: \ -\omega_1^2/k_1^2(3/2\alpha_1-2\alpha_2+\alpha_4)-(\alpha_2+\alpha_3)/2 \\ &\quad -2\omega_Q\omega_1/k_1^2\beta\pm ik_1 \end{aligned} \tag{20}$$

and

$$\begin{aligned} B_{\pm 1}&: \ -(\gamma_1+\gamma_2+\gamma_3+\gamma_4)/4+\omega_Q/k_1(\gamma_1-\gamma_2-\gamma_3 \\ &\quad +\gamma_4)/4-\omega_1/k_1\beta\pm ik_2, \\ B_{\pm 2}&: \ -(\gamma_1+\gamma_2+\gamma_3+\gamma_4)/4-\omega_Q/k_1(\gamma_1-\gamma_2-\gamma_3 \\ &\quad +\gamma_4)/4+\omega_1/k_1\beta\pm ik_3. \end{aligned} \tag{21}$$

In the $T_{1\rho}$ experiments, the relaxation rate of the satellites (at frequencies $\pm k_1$) is readily identified with the rate of the operators $A_{\pm 3}$. The rates of the two satellite pairs at frequencies $\pm k_2$ and $\pm k_3$ ($T_{2\rho}$ experiments) are given by the rates of the operators $B_{\pm 1}$ and $B_{\pm 2}$, respectively. However, satellites are liable to line-broadening by rf field inhomogeneity effects and/or a possible distribution in static quadrupolar coupling. Accordingly, their widths have little practical value.

In the $T_{1\rho}$ experiments a central line is observed which is not dephased by an inhomogeneous ω_Q or B_1 (apart from their effect on the relaxation rate). The relaxation behavior of this central line is related to the relaxation of

the operators A_1 and A_2 and is sensitive to the spectral density at frequencies k_1, ω_O, and $2\omega_O$. These operators are coupled, and, in principle, the relaxation is biexponential. The amplitudes and rates of both components have to be determined by numerical integration of the master Eq. (16). It was numerically checked that for any reasonable set of experimental parameters the amplitude of one component is negligibly small and the relaxation is quasiexponential. The full time-evolution matrix in the approximate eigenoperator representation shows that the operators A_1 and A_2 are decoupled in two limiting cases, i.e., if the spectral densities $J_1(\omega_O)$ and $J_2(2\omega_O)$ are negligibly small with respect to the low frequency contribution $J_0(k_1)$ and/or if $J_1(\omega_O)=J_2(2\omega_O)$. These situations are experimentally often met.

If the operators A_1 and A_2 are decoupled, the relaxation of the central line is purely exponential. The rate is given by the diagonal element corresponding to the operator A_2. Accordingly, in the $T_{1\rho}$ experiments the rate of the central line (denoted by superscript c) reads

$$R^c_{1\rho}=6\omega_1^2/k_1^2J_0(k_1)+[3+2\omega_1^2/k_1^2]J_f,$$
$$J_f=J_1(\omega_O)=J_2(2\omega_O). \tag{22}$$

The relaxation rate is sensitive to the spectral density at frequency k_1, which reduces to $2\omega_1$ if the static quadrupolar Hamiltonian is neglected. Moreover, this spectral density is weighed by the factor $6\omega_1^2/k_1^2$. In the conventional $T_{1\rho}$ experiment without coherence transfer, the relative amplitude of the central line is given by $4\omega_1^2/k_1^2$ (see Table II). In the limit $\omega_1 \gg \omega_Q$ this relative amplitude reduces to unity and the density operator relaxes according to Eq. (19).

To illustrate the relaxation behavior of the central line, a numerical example is presented. Under the condition $\omega_O\tau_c \gg 1$, the high frequency contributions $J_1(\omega_O)$ and $J_2(2\omega_O)$ are immaterial. The spectral density $J_0(k_1)$ is taken to be a Lorentzian

$$J_0(k_1)=3/40(e^2qQ/\hbar)^2\tau_c/(1+k_1^2\tau_c^2) \tag{23}$$

with e^2qQ/h the coupling constant of the fluctuating quadrupolar interaction. The relaxation rate vs $\omega_1/2\pi$ is depicted in Fig. 3 for a number of correlation times. The other parameters are as in Fig. 1. The approximate solution Eq. (22) is indiscernible from the rate obtained from the numerically solved time-evolution Eq. (16) (the linewidths are much smaller than the frequency k_1). For $\omega_1\tau_c \ll 1$, the rate increases with increasing spin-lock field strength according to $(6\omega_1^2/k_1^2)$ $[3/40(e^2qQ/\hbar)^2\tau_c]$ and eventually levels off at 3/2 $[3/40(e^2qQ/\hbar)^2\tau_c]$. For longer correlation times, i.e., $\omega_1\tau_c \approx 1$, the rate displays a maximum due to the spectral density dispersion. The position of this maximum depends on the value of the correlation time and/or the static quadrupolar interaction. The limiting behavior Eq. (19) is also displayed in Fig. 3. For small spin-lock field intensities the static quadrupolar Hamiltonian can clearly not be neglected. The limiting behavior is recovered, if ω_1 exceeds, say, five times ω_Q.

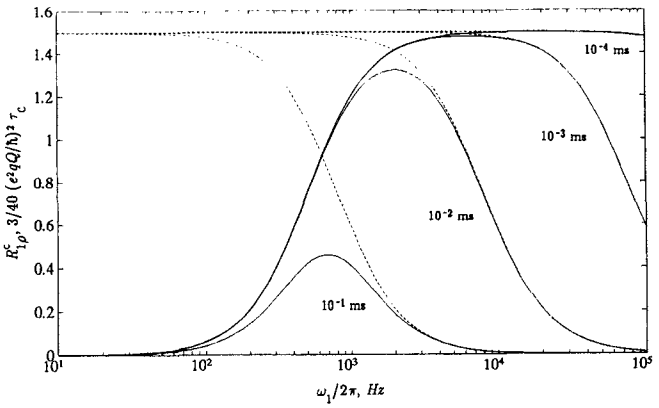

FIG. 3. The full curves represent the $T_{1\rho}$ relaxation rate Eq. (22) of the central line vs the spin-lock field strength $\omega_1/2\pi$. The dashed curves represent the limiting behavior Eq. (19) under the neglect of the static quadrupolar Hamiltonian. The various correlation times are indicated in the figure and the other parameters are as in Fig. 1.

EXPERIMENT

Experiments were performed on a Bruker AM-200 spectrometer equipped with a 4.7 T superconducting magnet and a fast recovery preamplifier. To achieve a homogeneous B_1 field, a homemade probe with a solenoid coil was used. To minimize dielectric heating during spin-locking, a Faraday shield was mounted around the sample inside the coil and at one side connected to ground. The temperature was controlled at 294 K by a fluid thermostat using Fluorinert grade FC-43 (3M Co.). The hard $(\pi/2)$ pulse duration was typically 11.5 μs, whereas the spin-lock field intensity was tuned between 0.37 and 4.08 kHz using a Bruker BFX-5 low power transmitter. (Methyl Sulfoxide)-d6 (DMSO-d6, Janssen) was dissolved in ZLi-1052 Merck liquid crystal. At a concentration of 5% by weight the deuterium signal shows a static quadrupolar splitting $2\omega_Q$ of the order of 2 kHz.[12] The carrier rf frequency was adjusted exactly on resonance.

The general spin-lock pulse sequence is represented by

$$(\pi/2)_{\phi+90}-(B_1)_\phi-(\pi/2)_{\phi'}\text{-detection.} \tag{24}$$

For $T_{2\rho}$ experiments the first preparation pulse is omitted. The final pulse is included for double-quantum filtration. For this purpose, the phase ϕ is stepped through the values 0°, 90°, 180°, and 270° while the receiver phase is alternated between 0° and 180°.[13] The phase ϕ' is set to the values 0° or 45° for selective detection of $\hat{T}_{22}(a)$ or $\hat{T}_{22}(s)$, respectively. For experiments without coherence transfer, the final detection pulse is omitted.

The double-quantum filtered $T_{1\rho}$ and $T_{2\rho}$ spectra are displayed in Figs. 4 and 5, respectively. The top spectra show the created and selectively detected $\hat{T}_{22}(s)[T_{1\rho}]$ and $\hat{T}_{22}(a)(T_{2\rho})$ coherences. For the bottom spectra, the detection was optimized for the unexpected $\hat{T}_{22}(a)$ and $\hat{T}_{22}(s)$ coherences, respectively. In the $T_{1\rho}$ experiment (Fig. 4), no $\hat{T}_{22}(a)$ signal could be detected. The $T_{2\rho}$ bottom spectrum shows a very small unexpected $\hat{T}_{22}(s)$ signal and an incomplete suppression of the $\hat{T}_{22}(a)$ coher-

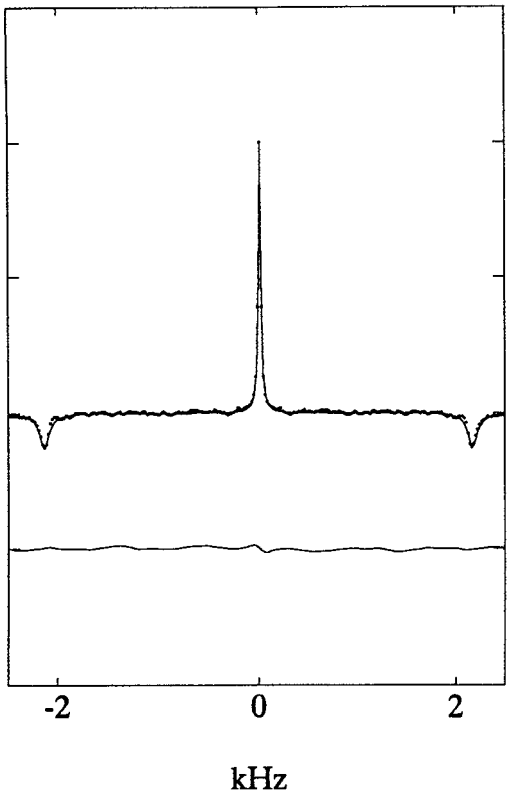

FIG. 4. Double-quantum filtered spectra resulting from the $T_{1\rho}$ experiments. The difference of the sections in the F_1 dimension (Fourier transform with respect to the spin-lock time) taken at the resonance positions of the two satellites in F_2 is displayed. The top spectrum shows the created and selectively detected $\hat{T}_{22}(s)$ signal, whereas for the bottom spectrum the detection was optimized for the (unexpected) $\hat{T}_{22}(a)$ coherence. The spin-lock increment time amounts 200 μs. The solid line is a simplex fit of the numerically solved time-evolution Eq. (16) with $\omega_1/2\pi=917$ Hz and $\omega_Q/2\pi=1135$ Hz. A 30 Hz Lorentzian line-broadening was applied to minimize truncation effects of the slowly relaxing central component.

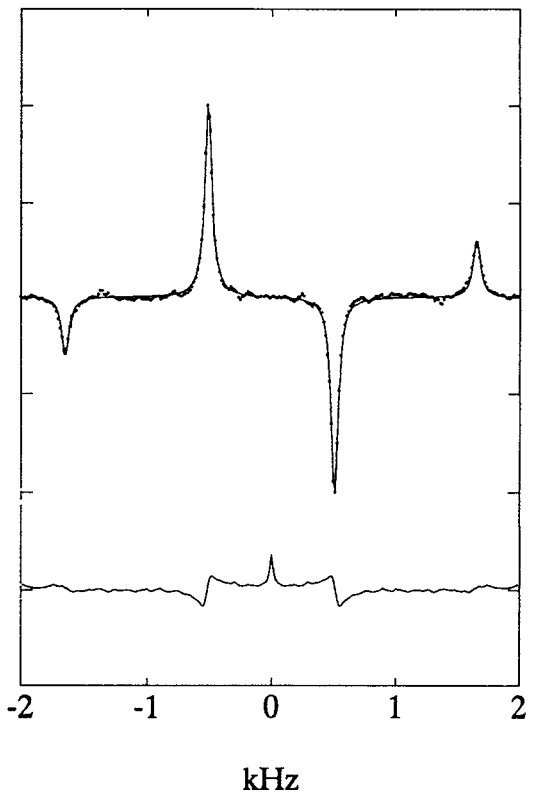

FIG. 5. Same as Fig. 4, but for $T_{2\rho}$ experiments. Here, the top spectrum represents the created and selectively detected $\hat{T}_{22}(a)$ signal. For the bottom spectrum the detection was optimized for the (unexpected) $\hat{T}_{22}(s)$ coherence. The latter spectrum shows an incomplete suppression of the $\hat{T}_{22}(a)$ signal (in dispersion mode) and a very small central feature due to the presence of $\hat{T}_{22}(s)$ coherence. These effects are due to pulse phase imperfections. The spin-lock increment time amounts 250 μs. The solid line is a simplex fit of the numerically solved time-evolution Eq. (17) with fit parameters and applied Lorentzian line-broadening as in Fig. 4.

ence. These effects are due to pulse phase imperfections. The top spectra are supplemented with a simplex fit of the numerically solved time-evolution Eqs. (16) and (17). The positions and relative amplitudes of the different resonances agree with the theoretical results. The spectral densities were obtained from separate relaxation measurements (see below) and not fitted to these data. The two satellite pairs of the $T_{2\rho}$ spectrum and the satellites of the $T_{1\rho}$ spectrum are broadened by 40 and 90 Hz, respectively, mainly due to B_1 field inhomogeneity.

The width of the central line has been investigated using the $T_{1\rho}$ experiment, but without coherence transfer [i.e., without the last pulse in Eq. (24)]. Now, the detected signal contains a mixture of $\hat{T}_{11}(a)$ and $\hat{T}_{21}(s)$ (the latter coherence is observable due to transverse relaxation during the detection period). The double-quantum coherence does not evolve into detectable magnetization. The sweep width in the F_1 dimension (i.e., the Fourier transform with respect to the spin-lock time) is adjusted to 33.3 Hz, and, hence, satellites are not observed. Moreover, the $\hat{T}_{21}(s)$ coherence does not show a significant central line (see Fig. 1). Accordingly, the detected signal essentially represents the central component of the $\hat{T}_{11}(a)$ coherence.

The spin-lock relaxation rate of the central line is depicted in Fig. 6 vs the ratio ω_1/ω_Q. The rate shows an increase with increasing rf field strength, but does not show a maximum. This indicates the absence of a spectral density dispersion in the present frequency range ($k_1=1.4$–8.2 kHz), i.e., $J_0(0)=J_0(k_1)$. The rates obtained from the numerically solved time-evolution Eq. (16) were fitted to the experimental values. For this purpose, the high frequency contributions $J_1(\omega_O)$ and $J_2(2\omega_O)$ were obtained from a Jeener–Broekaert experiment.[1,2] The values are $J_1(\omega_O)=0.95\pm0.02$ s^{-1} and $J_2(2\omega_O)=0.89\pm0.02$ s^{-1}. The spin-lock field strength as well as the static quadrupolar coupling constant were obtained from the resonance positions in the double-quantum filtered $T_{2\rho}$ spectrum. The solid line in Fig. 6 represents the simplex fit with only one adjustable parameter, i.e., $J_0(0)=J_0(k_1)=1.28\pm0.15$ s^{-1}. There is excellent agreement.

CONCLUSIONS

Differential equations were derived which describe the dynamics of spin $I=1$ nuclei in the presence of a rf field

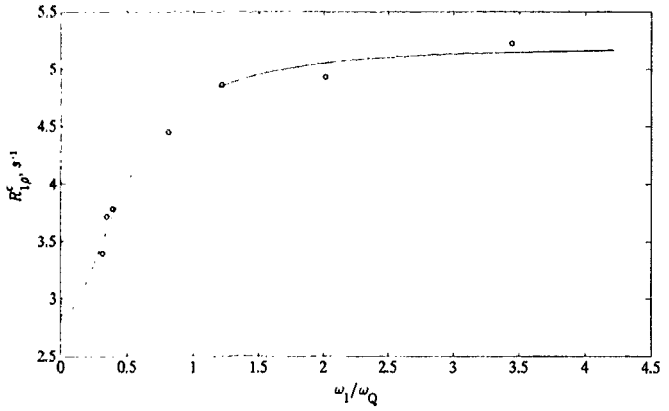

FIG. 6. (○) Experimentally observed $T_{1\rho}$ relaxation rate of the central component of the $\hat{T}_{11}(a)$ coherence vs the ratio ω_1/ω_Q. (—)Theoretical result from the numerically solved time-evolution Eq. (16) with $J_1(\omega_O)=0.95\pm0.02\ s^{-1}$, $J_2(2\omega_O)=0.89\pm0.02\ s^{-1}$, and $J_0(0)=J_0(k_1)=1.28\pm0.15\ s^{-1}$ (fitted). Experimental parameters, $\omega_Q/2\pi=1185$ Hz and a spin-lock increment time of 30 ms. The static quadrupolar constant is somewhat higher compared to the value observed in the double-quantum filtered experiments (Fig. 5) due to a slightly different DMSO-d6 concentration.

and both a static and fluctuating quadrupolar interaction. If relaxation effects are included, the time-evolution cannot be solved in analytical form. However, approximate solutions were obtained under the assumption that the linewidths are much smaller than the characteristic line-splitting. The relaxation rate of the central component (the conventional $T_{1\rho}$ relaxation rate) increases with increasing ratio ω_1/ω_Q and eventually levels off for $\omega_1 \gg \omega_Q$. The rate is sensitive to the value of the spectral density function at frequency $k_1 = \sqrt{\omega_Q^2+4\omega_1^2}$ and shows a maximum in the presence of a slowly fluctuating quadrupolar interaction (i.e., low frequency molecular motion). The limiting relaxation behavior under neglect of the static quadrupolar Hamiltonian is recovered if ω_1 exceeds, say, five times ω_Q.

Experiments were performed on DMSO-d6 in liquid crystal ZLi 1052. The selective creation of $\hat{T}_{22}(s)$ and $\hat{T}_{22}(a)$ multipolar states in $T_{1\rho}$ and $T_{2\rho}$ experiments, respectively, is demonstrated. The spin-lock field strength dependence of the relaxation rate of the central component of the spin-locked magnetization $[\hat{T}_{11}(a)]$ has been measured and agrees with the theoretical results. The central component is not inhomogeneously broadened due to an inhomogeneous B_1 and/or ω_Q, i.e., apart from their explicit effect on the relaxation rate.

The present contribution expands the range of applications for relaxation studies in systems in which the quadrupolar interaction is not completely averaged by molecular motion. Apart from low molecular weight liquid crystals, these systems include solid state molecular crystals and liquid crystal polymers. The spin-lock experiments may provide information regarding low frequency collective motion, e.g., director fluctuations and hydrodynamic modes.[14]

Note added in proof. Matrices similar to Eqs. (10) and (11) have been reported by Barbara.[15]

[1] R. R. Vold, in *Nuclear Magnetic Resonance of Liquid Crystals*, edited by J. W. Emsley (Reidel, Dordrecht, 1985).
[2] J. Jeener and P. Broekaert, Phys. Rev. **157**, 232 (1967).
[3] J. S. Blicharski, Acta Phys. Pol. A **41**, 223 (1972); Can. J. Phys. **64**, 733 (1986).
[4] J. R. C. van der Maarel, J. Chem. Phys. **91**, 1446 (1989).
[5] J. R. C. van der Maarel, J. Chem. Phys. **94**, 4765 (1991).
[6] G. J. Bowden, W. D. Hutchinson, and F. Separovic, J. Magn. Reson. **79**, 413 (1988).
[7] S. Vega and A. Pines, J. Chem. Phys. **66**, 5624 (1977).
[8] H. A. Buckmaster, R. Chatterjee, and Y. H. Shing, Phys. Status Solidi A **13**, 9 (1972).
[9] G. J. Bowden and W. D. Hutchinson, J. Magn. Reson. **67**, 403 (1986).
[10] A. Abragam, *Principles of Nuclear Magnetism* (Oxford University, Oxford, 1961).
[11] J. P. Jacobsen, H. K. Bildsøe, and K. Schaumburg, J. Magn. Reson. **23**, 153 (1976).
[12] S. Wimperis and G. Bodenhausen, Chem. Phys. Lett. **132**, 194 (1986).
[13] R. R. Ernst, G. Bodenhausen, and A. Wokaun, *Principles of Magnetic Resonance in One and Two Dimensions* (Oxford University, Oxford, 1987).
[14] N. Heaton, D. Reimer, and G. Kothe, Chem. Phys. Lett. **195**, 448 (1992).
[15] T. M. Barbara, J. Magn. Reson. **67**, 491 (1986).